ELSEVIER

Journal of Organometallic Chemistry 566 (1998) 225–235

Journal of Organometallic Chemistry

Matrix isolation Raman spectroscopy and photochemistry of $(\eta^5\text{-}C_5H_5)(OC)_2Fe–SiH_2R$ (R = H, CH_3) in comparison with density functional calculations

Claudia Fickert [a], Volker Nagel [a], Wolfgang Kiefer [a,*], Stephan Möller [b], Heinrich Jehle [b], Wolfgang Malisch [b], Ralf Stowasser [c], Gerhard Bringmann [1,c]

[a] *Institut für Physikalische Chemie, Universität Würzburg, Am Hubland, D-97074 Würzburg, Germany*
[b] *Institut für Anorganische Chemie, Universität Würzburg, Am Hubland, D-97074 Würzburg, Germany*
[c] *Institut für Organische Chemie, Universität Würzburg, Am Hubland, D-97074 Würzburg, Germany*

Received 14 April 1998

Abstract

The compounds $(\eta^5\text{-}C_5H_5)(OC)_2Fe–SiH_2R$ with R=H (**1**) and CH_3 (**2**) have been isolated in krypton or nitrogen matrices and subsequently detected by Raman spectroscopy, followed by a detailed vibrational analysis. To study the photochemistry of the iron silyl complexes **1** and **2**, Raman spectra were also taken after UV irradiation. Resonance Raman spectroscopy enabled the detection of newly generated species in low concentrations. Due to the observed differences in the spectra, a reaction mechanism for the photochemical conversion of **1** and **2** in matrices is suggested. The experimental spectra of **1** are compared with the vibrational data of density functional calculations. These calculations propose a CO-loss product with a (Fe, H, Si) three-centre bond as a stable intermediate for the photochemical conversion of **1**. Infrared measurements confirm the photochemical CO elimination.

Keywords: Matrix isolation; Raman spectroscopy; Silyl metal complexes; Photochemistry; Density functional theory

1. Introduction

Silicon-transition metal complexes represent reactive intermediates in a number of catalytic transformations [1]. Since the preparation of the first stable example of $Cp(OC)_2Fe–SiMe_3$ by Piper et al. in 1956 [2] silyl derivatives of nearly all transition metals have been synthesised [3]. In this context, SiH_3-complexes are of special interest, as they show high reactivity with respect to insertion reactions into the Si–H–bond [4] and are attractive starting materials for the synthesis of metallo-silicides via MOCVD [5]. We have established a simple access to SiH_3-complexes of the chromium [6] and iron [7] series and characterised these species extensively by structural and spectroscopic analyses, especially by Raman spectroscopy and vibrational analysis of the transition metal bonded silyl groups [6,8]. The calculated force fields and potential energy distribution demonstrated the complicated vibrational behaviour as well as the metal-silicon bond strength and the influence of the remaining ligands. A complete normal coordinate analysis (NCA) was carried out for $Cp(OC)_2Fe–SiH_3$ ($Cp=\eta^5\text{-}C_5H_5$), which includes the whole Cp ligand [9,10].

This species and related complexes are photochemically active with respect to CO-elimination, a behaviour that was used for modifying the transition metal fragment by CO/PR_3-exchange ([7]b). The principles of photochemistry of monosilyl or disilanyl complexes have been studied so far only for $Cp(OC)_2Fe\text{-}SiMe_3$

* Corresponding author. Tel.: +49 931 8886330; fax: +49 931 8886332; e-mail: wolfgang.kiefer@mgroe.uni-wuerzburg.de
[1] Also corresponding author.

0022-328X/98/$19.00
PII S0022-328X(98)00760-8

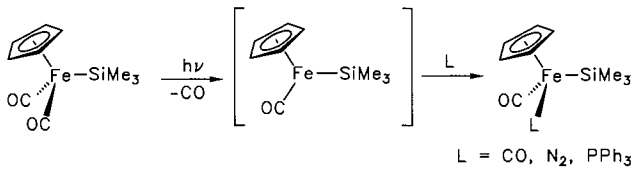

Scheme 1.

and $Cp(OC)_2Fe–Si_2Me_5$, respectively, by isolating the reactive intermediates in low-temperature frozen gas matrices for spectroscopic characterisation [11,12]. As demonstrated for the monosilyl complex, the primary photolysis-product is the 16-electron species $[Cp(OC)Fe–SiMe_3]$, which spontanously reacts with free CO or other potential ligands (e.g. N_2, PPh_3) to form the 18-electron complexes $Cp(OC)(L)Fe–SiMe_3$ Scheme 1 [12].

In contrast, the decarbonylated intermediate of $Cp(OC)_2Fe–Si_2Me_5$ shows intramolecular oxidative addition of the Si–Si bond to the metal, yielding the silyl(silylene)-iron complex $[Cp(OC)Fe(=SiMe_2)SiMe_3]$ Scheme 2 [12].

In this paper, we describe the use of Raman spectroscopy in combination with the matrix isolation technique for the analysis of the photochemistry of $Cp(OC)_2Fe–SiH_2R$ with R=H (**1**) and CH_3 (**2**). In contrast to the above-mentioned methyl-substituted derivatives, **1** and **2** contain a hydrogen ligand that can be easily transferred to the metal centre. This process should lead to a silylene complex proposed as an intermediate for several metal-catalyzed reactions of organosilanes, but proved only by a few stable examples [13,14].

2. Experimental

2.1. Preparation

The silyl complexes were synthesised by standard procedures [7,15].

2.2. Matrix isolation Raman and IR spectra

The matrix isolation apparatus [16] consisted of a cryocooler (CTI-Cryogenics, model 22C) and a turbopumping unit (Pfeiffer/Balzers, TPH 170). The latter guarantees that the pressure was in the region of 10^{-7} and 10^{-8} mbar. Clear and glassy matrices were prepared by using the 'slow-spray-on' technique [17]. The sample material was heated in a 'Knudsen cell' at 32°C. Afterwards, the gas was directly mixed with the matrix gas (krypton or nitrogen) in a heated nozzel, from where it was deposited on a highly polished gold plated copper head at 18–20 K.

For Raman excitation, the 647.1 nm line of a krypton ion laser (Spectra Physics, model 2025) or the 514.5 nm line of an argon ion laser (Spectra, model 165) were used. The laser beam was focussed on the matrix layer in an 30° angle to the target. The scattered light was dispersed by means of a double monochromator (Spex, model 1404) and the signal was detected by a CCD camera system (Photometrics, Spectra 9000). A resolution of 3 cm^{-1} was chosen for all spectra. Data acquisition and spectra analysis were performed by a commercial software package (MAPS, Photometrics) [18].

For IR absorption spectra, the matrix isolation apparatus was modified by a sapphir target and the cryo head was equiped with CsI windows. The measurments were carried out with a FT-IR spectrometer (Bruker IFS 120-HR) supplied with a Ge/KBr beamsplitter and a HgCdTe detector. A spectral resolution of 3 cm^{-1} and 50 scans per measurement were chosen.

For the UV irradiation, either an argon ion laser (Spectra, model BeamLok 2085), operating multiline within a wavelength range of 333 to 364 nm and 1–3 W laser power, or a krypton ion laser (Spectra, model 2025) in the 337–356 nm range and 100 mW laser power were used.

2.3. UV/VIS spectra

For UV/VIS spectra, the compounds **1** and **2** were disolved in dry benzene and handled under Ar atmosphere. The solutions were measured in quartz cells with a Perkin–Elmer Lambda 19 spectrometer.

2.4. Computational details of density functional calculations

For the following investigations, density functional (DF) methods were used, because of their moderate demand on CPU time (scaling factor $N^{2.2-3}$ with N basis functions, instead of N^4 for standard-HF-ab-initio-methods) and, as shown in the literature, because of

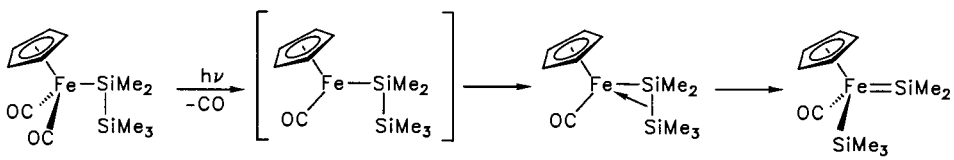

Scheme 2.

their capability to describe transition metal complexes in good agreement with experimental data [19]. DF calculations were performed on CRAY T90 computers by means of DGAUSS 3.0 [20,21]. The DF theory is based on the theorem of Hohenberg and Kohn [22], which states that the groundstate energy $E[\rho]$ of a system is an exact functional of the electron density ρ:

$$E[\rho] = T[\rho] + U[\rho] + E_{xc}[\rho],$$

in which T is the kinetic energy of non-interacting electrons, U the Coulomb potential, and E_{xc} the exchange correlation energy. For the calculation of the exchange correlation energy, the BP and BLYP functionals were used. All calculations were performed using the DZVP [23,24] basis set. The electronic density and the exchange correlation potential were fitted with a triple-zeta A1 [23,24] set. The ground state structures and the vibrational frequencies were determined by the standard techniques implemented in DGAUSS.

3. Results and discussion

The photochemical studies in low temperature matrices require a detailed analysis of the ferrio-silanes **1** and **2**. Hence, the following discussion starts with a Raman spectroscopic characterisation of the matrix isolated complexes **1** and **2**. The vibrational assignments were established according to earlier studies [9,10,25]. Density functional (DF) calculations of **1** support this investigation. The quality of the calculated data will be shown by a comparison with the experimental data. The following analysis of the irradiation experiments of matrix isolated **1** and **2** includes DF calculations of the reaction intermediate characterised by vibrational data.

3.1. Raman spectra of matrix isolated *1* and *2*

The compounds **1** and **2** were isolated in krypton or nitrogen matrices at 18 K and analysed by Raman spectroscopy with $\lambda_0 = 647.1$ and 514.5 nm excitation. These wavelengths were chosen, because they are located in the off-resonance region for both substances. This can be seen for **2** in the absorption spectrum shown in Fig. 1. Due to this, the spectra measured with $\lambda_0 = 647.1$ and 514.5 nm are identical and show no enhancement effect of particular Raman bands. Furthermore, no differences between Kr or N_2 matrices were observed.

The high quality of the matrix layers enabled polarised Raman measurements, which allowed the assignment of symmetric vibrations. The spectra of **2** with parallel and perpendicular polarisation are represented in Fig. 2 (spectrum B and C, respectively). Band positions, relative intensities, depolarisation ratios, and possible assignments for **1** and **2** are listed in Table 1 together with the vibrational data of **1** from density functional calculations, which will be discussed in Section 3.2.

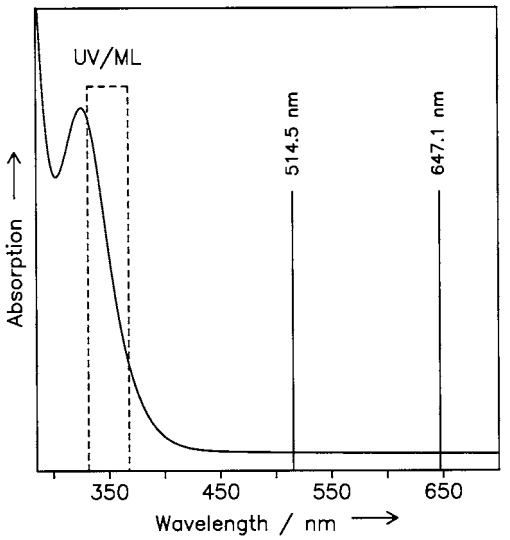

Fig. 1. UV/VIS absorption spectrum of $Cp(OC)_2Fe–SiH_2Me$ (**2**) in benzene, with mark of the Raman excitation wavelength and the spectral region (UV/ML = UV multiline) for the photochemical investigations.

Due to the small differences of the molecular framework, the Raman spectra of **1** (spectrum A in Fig. 2) and **2** (spectrum B in Fig. 2) look very similar. The spectra are dominated by the signals of the Cp ring breathing mode at 1115 cm^{-1} as well as the (FeCp) and (Fe–Si) stretching vibrations between 300 and 400 cm^{-1}. The antisymmetric and symmetric ν(SiH) modes are observed as a broad superimposed band around 2100 cm^{-1}. Between 1950 and 2010 cm^{-1}, the two (CO)

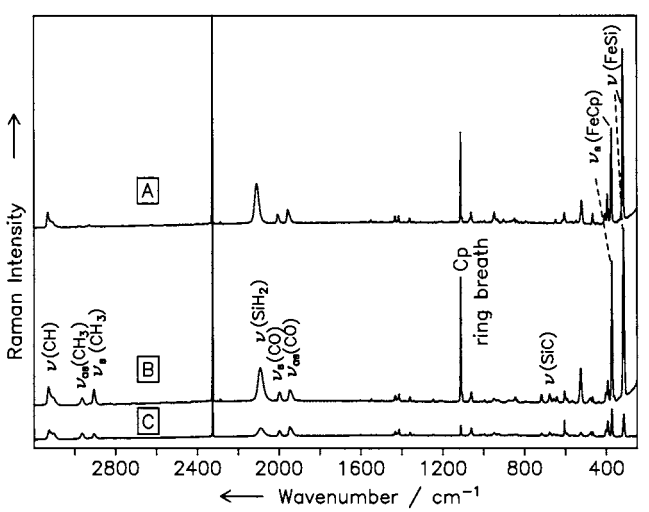

Fig. 2. Raman spectra of $Cp(OC)_2Fe–SiH_3$ (**1**) (spectrum A) and $Cp(OC)_2Fe–SiH_2Me$ (**2**) (B: parallel polarisation; C: perpendicular polarisation) in N_2 matrices at 18 K with $\lambda_0 =$ 514.5 nm.

Table 1
Raman data (wavenumber $\tilde{\nu}$ in cm^{-1}) of matrix isolated **1** and **2** compared with DF calculations of **1**

$Cp(OC)_2Fe-SiH_2R$ R=H (**1**)						R=CH_3 (**2**)	
Raman N_2-Matrix	DGAUSS calculations[a] BP/DZVP		BLYP/DZVP		Assignment	Raman N_2-Matrix	Assignment of (Si–R) modes
$\tilde{\nu}$	$\tilde{\nu}$	$\Delta\tilde{\nu}$	$\tilde{\nu}$	$\Delta\tilde{\nu}$		$\tilde{\nu}$	
3134 m	3205	+71	3194	+60	ν_s(CH)	3132 m/p	
3127 sh[b]	3192	+65	3183	+56	ν_{as}(CH)	3123 sh[b]	
	3192	+65	3181	+54			
3110 sh[b]	3183	+73	3172	+62	ν_{as}(CH)	3106 sh[b]	
3093 sh[b]	3178	+85	3171	+61		3094 sh[b]	
						2967 w	$\nu_{as}(CH_3)$
						2909 m/p	$\nu_s(CH_3)$
2113 s	2164	+51	2162	+49	ν_s(SiH)	2098 m/p	
2104 sh[b]	2145	+43	2141	+37	ν_{as}(SiH)	2088 sh[b]	
	2140	+36	2137	+33			
2009 w	2003	−6	1975	−34	ν_s(CO)	2002 w	
1960 m	1966	+6	1939	−21	ν_{as}(CO)	1951 w	
1434 w	1440	+6	1440	+6	ν_{as}(CC)	1435 w	
1417 w	1415	−2	1414	−3	ν_{as}(CC)	1416 w	
	1379		1364		ν_{as}(CC)		
1364 w	1373	+9	1358	−6	ν_{as}(CC)	1364 w	
	1255		1266		$\delta_{s/ip}$(CH)		
						1249 vw	$\delta_s(CH_3)$
1115 vs	1114	−1	1101	−14	Cp ring breathing	1115 vs/p	
1108 sh						1108 sh	
1073 sh						1087 vvw	
1063 w	1053	−10	1052	−11	$\delta_{as/ip}$(CH)	1063 w	
	1048		1048		$\delta_{as/ip}$(CH)		
1017 vvw	1014	−3	1011	−6	$\delta_{as/ip}$(CH)	1019 vvw	
999 vvw	994	−5	989	−10	$\delta_{as/ip}$(CH)	999 vvw	
950 w	956	+6	950	0	$\delta_{as/op}$(CH)	953 vw	
	946				$\delta_{as/op}$(CH)		
	936		942		$\delta_{as}(SiH_2)$		
			936		δ_{as}(SiH)		
935 vw	926	−9	931	−4	$\delta_{as}(SiH_2)$	933 vw	
905 vw	886	−19	892	−13	$\delta_s(SiH_3)$		
						881 vvw	
852 vw	862	+10	854	+2	$\delta_{as/op}$(CH)	849 vw/p	
	846				$\delta_{as/op}$(CH)		
			844		$\delta_{as/op}(CH)+\delta_{as/ip}(CCC)$		
841 vw	840	−1	838	−3	$\delta_{as/op}$(CH)	840 vw	
	833		831		$\delta_{as/op}(CH)+\delta_{as/ip}(CCC)$		
	824		817		$\delta_{s/op}$(CH)		
						720 w/p	
						680 w/p	ν(Si−C)
650 vw	663	+13	645	−5	$\delta_{s/ip}$(FeCO)	661 vw	
	627				$\delta_{as/ip}$(FeCO)	646 vw/p	
615 sh	611	−4			$\delta_{s/op}$(FeCO)	608 w	
608 vw	605	−3			δ_{op}(CCC)		
			602		$\nu_{as}(FeC_2)$	594 vw	
579 vvw	585	+6	598	+19	δ_{op}(CCC)		
			592		δ(FeSiH)+$\omega(FeC_2)$		
			577		$\delta_{as/op}$(CCC)	574 vvw	
567 vvw	578	+11	568	+1	δ(FeSiH)		
549 vw	528		521		$\tau(SiH_2)+\tau(FeC_2)$		
523 m	531	+8	507	−16	$\nu_s(FeC_2)$	528 m/p	
	513				$\nu_{as}(FeC_2)$		
			502		$\tau(SiH_2)+\nu_{as}(FeC_2)$	480 vw	
469 w	475	+6	460	−9	$\tau(FeC_2)$	470 vw	
446 vvw						439 vvw	

Table 1 (Continued)

$Cp(OC)_2Fe–SiH_2R$ R=H (**1**)						R=CH_3 (**2**)	
Raman N_2-Matrix	DGAUSS calculations[a] BP/DZVP		BLYP/DZVP		Assignment	Raman N_2-Matrix	Assignment of (Si–R) modes
$\tilde{\nu}$	$\tilde{\nu}$	$\Delta\tilde{\nu}$	$\tilde{\nu}$	$\Delta\tilde{\nu}$		$\tilde{\nu}$	
409 w	405	−4	376	−33	ν_{as}(CpFeSi)	405 w	
397 m	386	−11	356	−41	ν_{as}(FeCp)	396 m	
377 vs	367	−10	340	−37	ν_s(FeCp)	375 vs/p	
322 vs	316	−6	294	−28	ν_s(CpFeSi)	318 vs/p	
216 vw	190	−26	181	−35	$\tau(SiH_3)$		
155 m	160	+5	159	+4	δ(CpFeSi)	202 m	
142 sh	148	+6	146	+4	δ(CpFeC)	147 sh	
125 m	125	0	123	−2	$\delta(C_2FeSi)$		
107 m	110	+3	106	−1	δ(CfeC)		
	99		95		$\tau(FeC_2)$		
	64		71		τ(FeCp)		

[a] $\Delta\tilde{\nu} = \tilde{\nu}$(calculation) − $\tilde{\nu}$(Raman observed).
[b] From band shape analysis.

stretching vibrations occur with relatively weak intensities. Spectrum B in Fig. 2 shows the characteristic vibrations for the methylated silyl complex **2**. The signal at 2967 cm^{-1} can be assigned to the antisymmetric, and the polarised band at 2909 cm^{-1} to the symmetric $\nu(CH_3)$ mode. The (CH_3) deformation is seen as a weak signal at 1249 cm^{-1}. Two polarised bands can be observed in the (Si–C) stretching region at 680 and 720 cm^{-1}.

3.2. Density functional calculations of structural and vibrational data of *1*

Comparing the data of the X-ray structure determination of $(\eta^5\text{-}C_5Me_5)(OC)_2Fe–SiH_3$ ([7]b) with the calculated parameters by DF methods for the Cp-substituted analogue shows a very good correlation of the different data sets (Table 2). While the angles fit nearly exactly ($\Delta = 0–6°$), an elongated Fe–CO and a shortened C–O bond length is observed, which although it is in contrast to the expected values due to the more electron-donating effect of the permethylated Cp-ligand, lies within the known region of these bonds.

The results of vibrational calculations of **1**, based on DF methods using BP and BLYP functionals with the DZVP basis set [23,24], are listed together with the experimental wavenumbers in Table 1. The calculated vibrations were visualised with the programm UniChem [21]. The vibrations were assigned based on these visualisations and not on a calculated potential energy distribution (PED), which could not be carried out with the program used. In an earlier normal coordinate analysis of **1**, a PED was calculated, which shows the percentage of different internal coordinates on particular vibrations [9].

Most interestingly, the strongest deviations $\Delta\tilde{\nu}$ between calculated data and experimental values are observed for modes with participation of hydrogen atoms. This can be attributed to difficulties in describing a hydrogen by a homogeneous electron density [20]. The deviation is 50–90 cm^{-1} in the ν(CH) region and 30–50 cm^{-1} in the $\nu(SiH_3)$ region. The best conformity between calculation and experimental data is observed for the ν(CC) modes of the cyclopentadienyl ligand. In most cases, the BP functional gives a much better agreement with the experimental data than the BLYP functional. For example, the deviation between calculated and experimental values of the ν(CO) modes is only ± 6 cm^{-1} for BP functional and approximately -20 cm^{-1} for the BLYP functional. For the interesting iron-ligand vibrations, the deviation between the BP calculated wavenumbers from the experimental data amount to a maximum of 20 cm^{-1}. It is important to mention that the good agreement between calculated

Table 2
Calculated structure parameters of **1** by DF methods compared with x-ray data of $(\eta^5\text{-}C_5Me_5)(OC)_2Fe–SiH_3$

	$Cp(OC)_2Fe–SiH_3$ (**1**)		$Cp^*(OC)_2Fe–SiH_3$
	BP/DZVP	BLYP/DZVP	X-ray data ([7]b)
Bond lengths (Å)			
Fe–Si	2.316	2.347	2.287
Fe–CO	1.758/1.756	1.776/1.774	1.813/1.773
C–O	1.175/1.175	1.176/1.176	1.034/1.127
Angles (°)			
Si–Fe–C	85.9/85.1	86.5/85.8	92.5/89.4
Fe–C–O	177.8/179.0	177.5/178.6	177.5/178.3
C–Fe–C	94.6	95.4	94.0

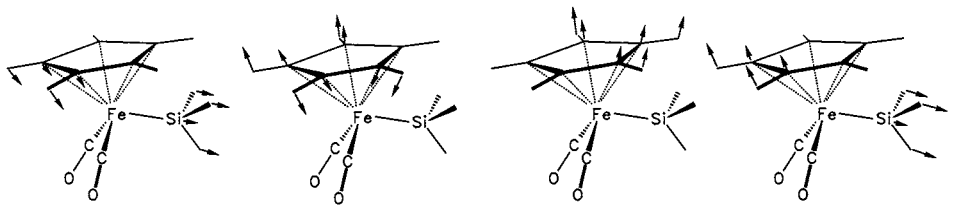

Fig. 3. Description of the (CpFeSi) stretching vibrations of $Cp(OC)_2Fe–SiH_3$ (**1**) and their calculated values using the BP functional.

values and experimental wavenumbers was, in contrast to former HF calculations [26], obtained without any empirical corrections. The especially interesting (Fe–Si) valence mode only differs about -6 cm^{-1} from the experimental data. The visualisation of this vibration shows a strong coupling with a symmetric (FeCp) stretching. Hence, this motion should be better described as a symmetric ν(CpFeSi) mode (see Fig. 3). The analogous antisymmetric vibration could be assigned to the weak signal at 409 cm^{-1}. The vibrations around 370 and 390 cm^{-1} are characterised by a higher (CpFe) stretching participation and, because of this, described as ν_s(CpFe) and ν_{as}(CpFe).

3.3. Photochemistry of matrix isolated *1*, Raman spectroscopic study and DF calculation

For the photochemical conversion of **1**, a reaction mechanism as shown in Scheme 3 is proposed. The photochemical ejection of one CO molecule forms the 16-electron species $[Cp(OC)FeSiH_3]$ (**II**). The α-H rearrangement leads to an intramolecular stabilisation of this intermediate. The reaction may stop with the formation of **III**, an intermediate with a (Fe, H, Si) three-centre bond or go further to the hydrido-silylene complex **IV**.

The proposed photochemical intermediates **II**–**IV** possess characteristic molecular units, which lead to characteristic vibrational modes. Therefore, a clear identification should be possible by means of Raman and IR spectroscopy. Due to the observation of Haynes et al. [12], the ν(CO) mode of **II** and **III** should appear at about 1925 cm^{-1} and of **IV** at about 1940 cm^{-1}. The higher [FeSi] bonding order in **III** and **IV** leads to a shift of the ν(FeSi) vibration to higher wavenumbers. In comparison to the shift observed between an iron-carbon single and an iron-carbon double bond ($HFe–CH_3$: 522 cm^{-1}; $Fe{=}CH_2$: 624 cm^{-1}) [27], the difference between the ν(Fe–Si) and the ν(Fe=Si) mode

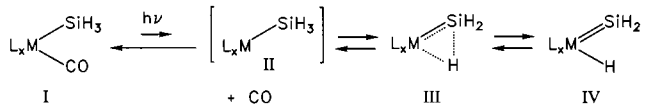

Scheme 3.

should amount approximatly 100 cm^{-1}. Complexes **III** and **IV** will also show the ν(SiH) modes at higher wavenumbers in comparison to **I** and **II**. An additional band should appear for the (FeH) stretching vibration. A complete migration of the silyl hydrogen atom to the iron centre in **IV** should be indicated by a signal at about 1835 cm^{-1} corresponding to the ν(FeH) of $Cp(OC)_2FeH$ [28]. The bonding situation in **III** is comparable with the agostic coordination of a [Si–H] unit like the η^2 coordination of SiH_4 in *cis*-$Mo(\eta^2$-$SiH_4)(CO)(Ph_2PC_2H_4PPh_2)$ ([29]a). Here the ν(MoHSi) mode was located at 1743 cm^{-1}. The ν(MoH) band was found at about 1800 cm^{-1} in the IR spectra of hydrido molybdenum complexes. Therefore, the signal of **III** was expected at about 1770 cm^{-1}. The vibrations between the iron centre and the cyclopentadienyl or the carbonyl ligand should also be affected. The Cp ring modes are relatively insensitive to the remaining complex fragment, and therefore, the Cp ring breathing can be used as internal standard. Free CO molecules in the matrix can be detected by their strong absorption in the IR spectrum at approximately 2139 cm^{-1} [12].

The photochemical conversion of **1** was initiated by irradiation of the matrix layer with an Ar ion laser as described above. After the irradiation the color of the layer changed from colorless to orange-red. The Raman spectra of matrix isolated **1** in N_2, which were detected before and after 15 minutes UV irradiation with 300 mW laser power are shown in Figs. 4 and 5. The same spectra are observed for krypton matrices, which exclude the possible CO/N_2 exchange in the nitrogen environment [12]. UV irradiation of matrix isolated **1** leads to an additional signal at 2181 cm^{-1} in the Raman spectra (see B and C in Fig. 4), which could be assigned to the (SiH) mode of a photochemical intermediate. The wavenumber of this (SiH) mode lies in the range observed for the terminal Si–H unit in the case of $[Cp_2Zr(\mu\text{-}H)(SiHPh_2)]_2^{2+}$ (2113 cm^{-1}) containing in addition an agostic Si–H bond ([29]b). The low signal to noise ratio in the spectra, which were taken after UV irradiation, can be attributed to the low laser power during the measurement. The UV irradiation caused a deterioration in the quality of the matrix layer. Due to this, the subsequent Raman measurements were carried out with a maximum laser power of only 5 mW. A

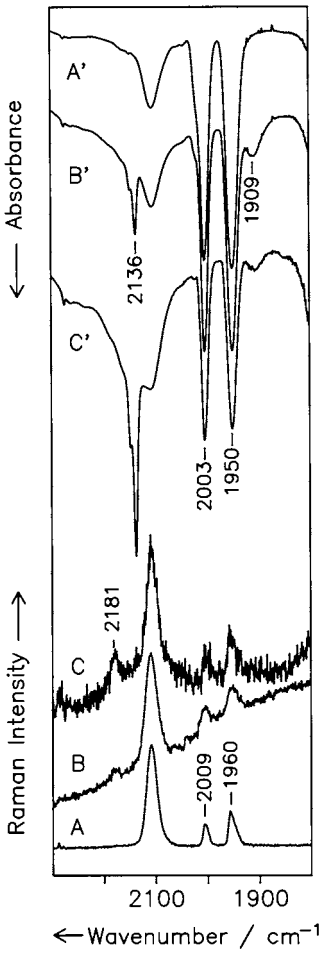

Fig. 4. Raman spectra of $Cp(OC)_2Fe–SiH_3$ (**1**) isolated in N_2 matrix at 18 K A: before photolysis with λ_0 = 514.5 nm (P = 50 mW), B: after 15 min UV irradiation (with 300 mW of an Ar^+ laser) with $\lambda_0 = 647.1$ nm ($P = 5$ mW), C: after 15 min UV irradiation (with 300 mW of an Ar^+ laser) with $\lambda_0 = 514.5$ nm ($P = 2$ mW) and IR spectra of **1** isolated in Kr/N_2 mixture at 18 K A′: before photolysis, B′: after 30 min UV irradiation (with 300 mW of an Ar^+ laser), C′: after 160 min UV irradiation (with 300 mW of an Ar^+ laser).

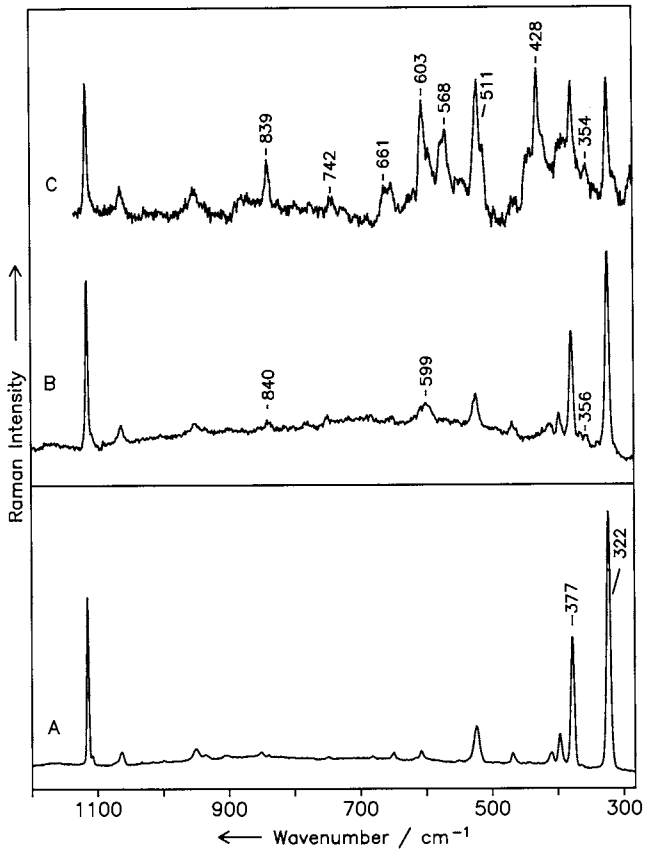

Fig. 5. Raman spectra of $Cp(OC)_2Fe–SiH_3$ (**1**) isolated in N_2 matrix at 18 K A: before photolysis with $\lambda_0 = 514.5$ nm ($P = 50$ mW), B: after 15 min UV irradiation (with 300 mW of an Ar^+ laser) with $\lambda_0 = 647.1$ nm ($P = 5$ mW), and C: after 15 min UV irradiation (with 300 mW of an Ar^+ laser) with $\lambda_0 = 514.5$ nm ($P = 2$ mW).

higher laser power leads to a damage of the matrix layer. IR experiments (see spectra A′–C′ in Fig. 4) give further information. After UV irradiation, an additional absorption could be observed at 2136 cm^{-1} in spectra B′ and C′. This indicates the formation of free CO molecules in the matrix. A further signal could be observed at 1909 cm^{-1}. The ν(CO) band of the photointermediate **II** and **III** are expected at lower wavenumber than the ν_{as}(CO) of **1** [12]. Therefore, the absorption at 1909 cm^{-1} could be assigned to the ν(CO) mode of a newly generated species. Neither the IR nor the Raman spectra show an additional signal in the ν(FeH) region.

Fig. 5 shows Raman spectra in the range of 200–1200 cm^{-1} before (spectrum A) and after UV irradiation (spectra B and C). Spectrum B was measured with $\lambda_0 = 647.1$ nm excitation and shows little differences in comparison to spectrum A. An increase in the irradiation time produced no further effects. The values of the additional bands are marked in spectrum B and listed in Table 4. The new signal at 356 cm^{-1}, between the strong ν_s(FeCp) and ν(FeSi) band of the educt **1**, could be attributed to the ν_s(FeCp) of an intermediate. Because of the small shift, this assignment is more probable than an alternative assignment to a ν(FeSi) mode of **III** or **IV**. The signals of the ν(FeSi) and ν_s(FeCp) mode show a decrease in intensity compared to the consistent intensity of the Cp ring breathing band. This observation indicates the reaction of **1** and the changed bonding situation in the photochemically generated intermediate.

The spectrum of the irradiated matrix layer is considerably changed by measurements using $\lambda_0 = 514.5$ nm excitation, since this wavelength is located in the absorption range of the newly generated species. This can be deduced from the color of the layer, which changed from colorless to red after the UV irradiation. The relative strong signals below 1000 cm^{-1} in the Raman spectrum C can be attributed to the resonance enhanced effects, which allow the detection of species in

Table 3
Calculated structure parameters of $Cp(OC)FeHSiH_2$ by DF methods

	$Cp(OC)FeHSiH_2$	
	BP/DZVP	BLYP/DZVP
Bond lengths (Å)		
Fe–Si	2.143	2.174
Fe–HSi	1.662	1.699
FeH–Si	1.698	1.675
Si–H	1.511/1.505	1.509/1.503
Fe–CO	1.757	1.777
C–O	1.178	1.179
Angles (°)		
C–Fe–Si	91.9	92.7
C–Fe–H	93.3	94.2
H–Fe–Si	51.1	49.4
Fe–H–Si	79.2	80.2
Fe–C–O	177.6	177.5

very low concentrations [30]. Spectrum C again shows a decrease of the ν(FeSi) band and a new signal at 354 cm^{-1}. Additionally, a new strong band can be seen at 428 cm^{-1}. This is the range, in which the (FeSi) stretching mode of the new species **III** or **IV**, with higher bond order between iron and silicon can be expected. Further strong signals appear in the region of the iron–carbonyl stretching and bending modes between 500 and 600 cm^{-1}. Moreover, some weak signals can be observed at 839, 742, and 661 cm^{-1} in the δ(SiH) region.

It should be further mentioned that **1** can react photochemically to the diiron complex $[CpFe(CO)_2]_2$, which can in turn react photochemically on to $[CpFe(CO)_3FeCp]$ in the timeframe of a Raman measurement when a wavelength of 514.5 nm is used. $[CpFe(CO)_3FeCp]$ possess a characteristic resonance Raman spectrum when excited with $\lambda_0 = 514.5$ nm [31,32], which was not observed during the matrix experiments above. Due to this, a reaction path of **1** reacting to $[CpFe(CO)_3FeCp]$ via $[CpFe(CO)_2]_2$ can be excluded in matrix.

DF calculations clearly indicate a CO-loss photoproduct with a (Fe, H, Si) three-centre bond as shown in Scheme 4.

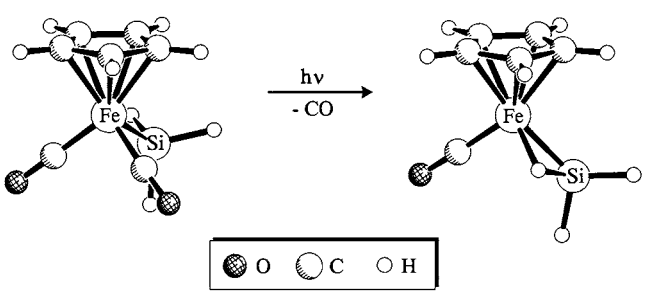

Scheme 4.

The parameters of the structure, which were calculated with the BP and the BLYP functional, are listed in Table 3. Both methods give equal changes in bond lengths and angles between the educt and the photoproduct structure. The transition from a [FeSi] single to a [FeSi] multiple bond leads to a shortening of 0.173 Å in the bond length. In comparison to the terminal hydrogen atoms, the bridging H atom is characterized by a longer [SiH] bond distance. The [C–Fe–Si] angle increases for the calculated photoproduct from 86 to 92°. The photoproduct possesses the same [FeC] and [CO] bond distances as the educt.

Additionally, calculations of vibrational wavenumbers were made to assist the interpretation of the Raman spectroscopic investigations. The calculated values of the characteristic vibrations are listed in Table 4. Experimental studies have shown, that the band position of the Cp ring breathing mode is virtually independent of the coordination sphere of the metal centre. The Cp ring breathing mode shows a difference of about 6 cm^{-1} between the educt and product in both, the BP and the BLYP calculations. Vibrations with participation of hydrogen atoms will not be discussed in detail, due to their relatively large deviation from the experimental data (Section 3.2). The (FeSi) stretching vibration of the product was calculated with the BP functional at 459 cm^{-1} and with the BLYP at 431 cm^{-1}. The values for the product are higher in wavenumber than the calculated ν_s(CpFeSi) mode of the educt **1** and lie in the expected range for [FeSi] multiple bonds. The Raman measurements after UV irradiation show a strongly enhanced signal at 428 cm^{-1} for the 514.5 nm excitation. Based on the calculations, this band can definitely be assigned to the ν(FeSi) mode of the newly generated **III**. The calculated value for the ν_s(FeCp) mode in **III** lies at lower wavenumbers than in the educt **1**. This is in good agreement with our expectations. The additional signal in the Raman spectra at approximately 355 cm^{-1} can be assigned to this mode. Further conformities are given in Table 4. Although the structural changes between the educt and the photoproduct are neglectable with regard to the [FeCO] unit, the vibrational calculations show the expected increasing value of the ν(FeC) mode in going from the educt to product. The ν(CO) mode of the product **III** was calculated at approximately 1963 cm^{-1} by using the BP functional or 1940 cm^{-1} for the BLYP functional. These values lie in the same region as the calculated values for the symmetric ν(CO) mode of the educt and are of higher wavenumber than expected. This depends on the deviation of the calculated structure from the structure in matrix. Therefore, the observed IR absorption at 1909 cm^{-1} thoroughly indicates the photochemical generation of **III** in the matrix.

Table 4
Calculated vibrational data of $Cp(OC)FeHSiH_2$ and Raman data of matrix isolated **1** and **2** after UV irradiation (wavenumber in cm^{-1})

Cp(OC)Fe-SiH_2 \ / H			$Cp(OC)_2FeSiH_3$ (**1**) after UV irradiation		$Cp(OC)_2FeSiH_2CH_3$ (**2**) after UV irradiation	
DGAUSS calculations Assignment	BP/DZVP	BLYP/DZVP	N_2 matrix $\lambda_0 = 647$ nm	N_2 matrix $\lambda_0 = 514$ nm	Kr matrix $\lambda_0 = 647$ nm	N_2 matrix $\lambda_0 = 514$ nm
ν(SiH)	2147	2149	2177 m	2182 m		2159 w
	2117	2118				
ν(CO)	1963	1940				
ν_s(FeHSi)	1662	1607				
			1467 vw			1043 vw
$\delta(SiH_2)$	949	960				1010 w/br
			840 vw	839 m	839 m	838 m
$\rho(FeH_{Si})$	762	782	748 vw	742 w		
$\omega(SiH_2)$	664	648		661 w		
					622 sh	626 vw
						618 w
ν(FeC)	591	576	599 w/br	603 s	597 m	603 s
δ(FeCO)	580	556		593 sh		
						572 s
$\delta(FeCO)+\delta(HSiH_{Fe})$	540	525		568 s/br 511 sh/m		568 s
$\rho(SiH_2)$	501	486		440 sh		
ν(FeSi)	459	431		428 vs		439 s
$\tau(SiH_2)$	416	401				429 m
ν_{as}(FeCp)	389	366		387 sh		388 sh
ν_s(FeCp)	340	335	356 vw	354 w	348 m	348 w
				313 sh		
			281 vw	287 w	281 w	

3.4. Photochemistry of matrix isolated *2*

The compound **2** possesses two different substituents coordinated to the silicon atom. Due to this situation, besides the α-H-transfer in analogy to **1** (pathway A) two further pathways can be discussed for the photochemical conversion of **2**, which are illustrated in simplified form in Scheme 5.

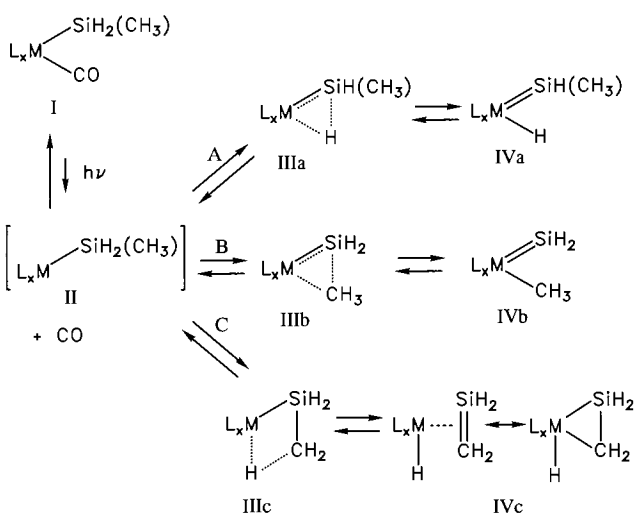

Scheme 5.

Reaction pathway **B** involves oxidative addition of the Si–C bond to the metal centre which should be less probable than pathway **A**. Additionally, Haynes et al. [12] could not observe an intramolecular stabilisation of $[Cp(CO)FeSiMe_3]$ in matrix. Only the exchange of one methyl group by a $[SiMe_3]$ function leads to an intramolecular stabilisation of $[Cp(OC)FeSiMe_2SiMe_3]$ by an α-$SiMe_3$ rearrangement. A further possibility for the photochemistry of **2** is a β-H rearrangement shown in pathway **C**. The spectroscopic identification of the intermediates **IIIa** and **IVa** are based on analogous considerations, which were discussed for **1**. A differentiation between **IIIa** and **IIIb** or **IVa** and **IVb** should be possible with the appearence of new signals for the (FeH) or (FeC) modes, respectively. For **IIIc** and **IVc**, wavenumber shifts in the ν(CH) and (SiC) modes are expected.

The Raman experiments of **2** were carried out analogously to the investigations of **1**. Fig. 6 shows the ν(SiH) and ν(CO) region of the Raman spectra of **2** before (spectrum A) and after UV irradiation (spectrum B and C). The new signal at 2159 cm^{-1} in spectrum B and C can be attributed to the ν(SiH) mode of a newly generated photoproduct like **IIIa** or **IVa**. The Raman spectra of the educts **1** and **2** possess a characteristic wavenumber shift of the ν(SiH) modes. The methyl

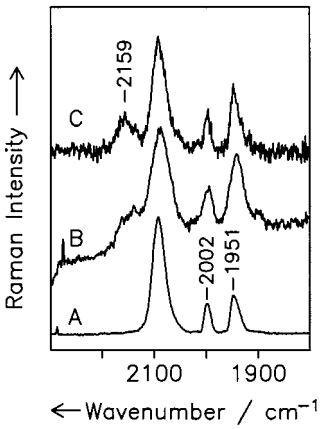

Fig. 6. Raman spectra of $Cp(OC)_2Fe–SiH_2Me$ (**2**) A: in N_2 matrix at 18 K before photolysis with $\lambda_0 = 514.5$ nm ($P = 50$ mW), B: in Kr matrix at 20 K after 60 min UV irradiation (with 50 mW of a Kr^+ laser) with $\lambda_0 = 647.1$ nm ($P = 15$ mW), and C: in N_2 matrix at 18 K after 15 min UV irradiation (with 300 mW of an Ar^+ laser) with $\lambda_0 = 514.5$ nm ($P = 3$ mW).

substitution of the silyl unit in **2** leads to a shift of approximately -16 cm^{-1}. The new Raman band at 2159 cm^{-1} in spectrum B and C (Fig. 6) also appeared at lower wavenumber than for **1** (2181 cm^{-1} in Fig. 4 B and C). The similar shift of these signals is evidence for a rearrangement equivalent to pathway **A** in Scheme 5. The detection of free CO molecules in the matrix after the UV irradiation was possible by means of IR experiments. Besides this, no further signals were observable in the ν(CO) range, which can characterise a newly generated photoproduct.

Fig. 7 shows the Raman spectra of matrix isolated **2** in the low wavenumber range before (spectrum A) and after UV irradiation (spectrum B and C). Spectrum B, which was taken after UV irradiation, with $\lambda_0 = 647.1$ nm, only shows a few additional bands besides the characteristic Raman features of **2** (see spectrum A). This can be explained with the equilibrium between the photochemical generation of the 16-electron complex **II** and a recombination to the starting compound **I** (**2**). Spectrum B shows a decreasing intensity for the ν(FeSi) and ν_s(FeCp) bands of the educt **2** and a new signal at 348 cm^{-1}, which can be attributed to the ν_s(FeCp) mode of the new species. A comparison with Raman spectra of the photoproduct of **1** in Fig. 5 B shows a wavenumber shift of approximately -8 cm^{-1} for this ν_s(FeCp) band. Further bands occur at 597 and 839 cm^{-1}.

Analogous to the irradiation of **1**, the orange-red color of the matrix layer indicates the photochemical reaction of **2**. Therefore, the Raman excitation with $\lambda_0 = 514.5$ nm leads to a resonance enhancement of several spectral bands in spectrum C of Fig. 7. Spectrum C shows a strong doublet at about 430 cm^{-1}, which can be assigned to the (FeSi) stretching mode of a newly generated photoproduct. Further bands occured in the ν(FeC) and δ(FeCO) region between 550 and 620 cm^{-1}. Two weaker signals were detected at 838 and 1010 cm^{-1}. Furthermore, the strong decrease in intensity of the ν(FeSi) band indicates a change of the iron silicon bonding behaviour, which also effects the [FeCp] bond. The ν_s(FeCp) mode of the photointermediate is observed at lower wavenumber (348 cm^{-1} in spectrum B and C of Fig. 7) than for the educt 2.

The UV irradiation of matrix isolated **1** and **2** leads to equivalent changes in the Raman spectra of both complexes. Therefore, the α-H rearrangement of **2** is more probable than the intramolecular stabilisation of **II** via an α-methyl or a β-H shift shown in Scheme 5.

4. Conclusions

The combination of matrix isolation techniques with Raman spectroscopy is a very attractive method for the determination of Si–H units attached to metal centres, concerning the bonding-mode in photochemically gen-

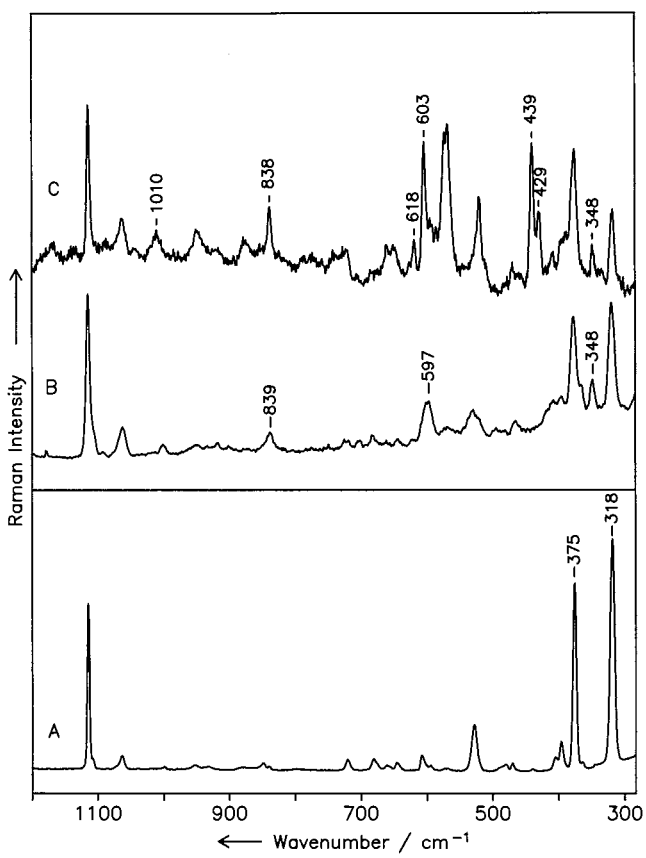

Fig. 7. Raman spectra of $Cp(OC)_2Fe–SiH_2Me$ (**2**) A: in N_2 matrix at 18 K before photolysis with $\lambda_0 = 514.5$ nm ($P = 50$ mW), B: in Kr matrix at 20 K after 60 min UV irradiation (with 50 mW of a Kr^+ laser) with $\lambda_0 = 647.1$ nm ($P = 15$ mW), and C: in N_2 matrix at 18 K after 15 min UV irradiation (with 300 mW of an Ar^+ laser) with $\lambda_0 = 514.5$ nm ($P = 3$ mW).

erated 16-electron intermediates. In this context it is of high interest, which kind of stabilisation the photolysis products of the iron complexes $Cp(OC)_2Fe–SiH_2–SiH_3$ and $Cp(OC)_2Fe–CH_2–SiH_3$, bearing a disilanyl or silylmethyl ligand, will undergo. This question will be the motivation to perform further matrix isolation experiments with these compounds.

Acknowledgements

We gratefully acknowledge financial support from the Deutsche Forschungs-gemeinschaft (Sonderforschungsbereich No. 347 'Selektive Reaktionen Metall-aktivierter Moleküle', projects B-1, B-2, and C-2) as well as the Fonds der Chemischen Industrie (financial support and a generous fellowship to R.S.). Thanks are also due to the Leibnitz–Rechenzentrum (München) and the Konrad–Zuse–Rechenzentrum (Berlin) for providing computational time on CRAY computers, and to P. Ruff (Rechenzentrum Würzburg) for helpful support.

References

[1] C.A. Recatto, Aldrichim. Acta 28 (1995) 85.
[2] T.S. Piper, D. Lemal, G. Wilkinson, Naturwissenschaften 43 (1956) 129.
[3] K. Horn, Chem. Rev. 95 (1995) 1317. T.D. Tilley, in: S. Patai, Z. Rappoport (Eds.), The Chemistry of Organic Silicon Compounds, Wiley Interscience, Chichester, 1989, Chapter 24.
[4] W. Adam, U. Azzena, F. Prechtl, K. Hindahl, W. Malisch, Chem. Ber. 125 (1992) 1409. W. Malisch, K. Hindahl, H. Käb, J. Reising, W. Adam, F. Prechtl, Chem. Ber. 128 (1995) 963. S. Möller, O. Fey, W. Malisch, W. Seelbach, J. Organomet. Chem. 507 (1996) 239. W. Malisch, S. Schmitzer, R. Lankat, M. Neumayer, F. Prechtl, W. Adam, Chem. Ber. 128 (1995) 1251. W. Malisch, R. Lankat, O. Fey, J. Reising, S. Schmitzer, J. Chem. Soc, Chem. Comm. (1995) 1917. W. Malisch, R. Lankat, S. Schmitzer, J. Reising, Inorg. Chem. 34 (1995) 5701.
[5] H. Suhr, Surf. Coat. Technol. 49 (1991) 223. F. Maury, Adv. Mater. 3 (1991) 542. T.T. Kodas, M.J. Hampden-Smith, in: The Chemistry of Metal CVD, VCH, Weinheim, 1994.
[6] W. Malisch, R. Lankat, S. Schmitzer, R. Pikl, U. Posset, W. Kiefer, Organometallics 14 (1995) 5622.
[7] (a) H.-U. Wekel, W. Malisch, J. Organomet. Chem. 264 (1984) C10. (b) W. Malisch, S. Möller, O. Fey, H.-U. Wekel, R. Pikl, U. Posset, W. Kiefer, J. Organomet. Chem. 507 (1996) 117.
[8] R. Pikl, U. Posset, S. Möller, R. Lankat, W. Malisch, W. Kiefer, Vibr. Spectrosc. 10 (1996) 161.
[9] T. Polzer, W. Kiefer, Asian J. Physics 6 (1997) 260.
[10] R. Pikl, C. Fickert, W. Kiefer, Trends Organomet. Chem. 2 (1997) 71.
[11] K.H. Pannell, J. Cervantes, C. Hernandez, J. Cassias, S. Vincenti, Organometallics 5 (1986) 1056.
[12] A. Haynes, M.W. George, M.T. Harward, et al., J. Am. Chem. Soc. 113 (1991) 2011.
[13] P.D. Lickiss, Chem. Soc. Rev. (1992) 272. S.D. Grumbine, T.D. Tilley, J. Am. Chem. Soc. 115 (1993) 7884. D.A. Straus, C. Zhang, G.E. Quimbita et al., J. Am. Chem. Soc. 112 (1990) 2673. M. Denk, R.K. Hayashi, R. West, J. Chem. Soc., Chem. Commun. (1994) 33.
[14] C. Zybill, H. Handwerker, H. Friedrich, Adv. Organometal. Chem. 36 (1994) 229.
[15] W. Malisch, W. Ries, Chem. Ber. 112 (1979) 1304.
[16] D. Gernet, W. Kiefer, Fresenius J. Anal. Chem. 362 (1998) in press.
[17] M.J. Almond, A.J. Downs, in: R.J.H. Clark, R.E. Hester (Eds.), Spectroscopy of Matrix Isolated Species, Advances in Spectroscopy, vol. 17, Wiley, Chichester, 1989, p. 15.
[18] MAPS, Spectroscopy Software for Windows, Photometrics GmbH, Version 1.0, Tuscon, AZ 85706.
[19] T. Ziegler, Chem. Rev. 91 (1991) 651.
[20] J. Andzelm, in: J. Labanowski, J. Andzelm (Eds), Density Functional Methods in Chemistry, Springer, New York 1991 and refs. therein.
[21] J. Andzelm, E. Wimmer, D.R. Salahub, in: D.R. Salahub, M.C. Zerner (Eds), The challenge of d and f Electrons: Theory and Computations, ACS Symposium Series, No. ~ 394, American Chemical Society, Washington, DC, 1989, p. 228, and refs. therein. DGauss is available as part of the UniChem software from Cray Research Inc., Eagan, MN.
[22] P. Hohenberg, W. Kohn, Phys. Rev. B 136 (1964) 864.
[23] J. Andzelm, E. Radzio, D.R. Salahub, J. Comput. Chem. 6 (1985) 520.
[24] N. Godbout, D.R. Salahub, J. Andzelm, E. Wimmer, Can. J. Chem. 70 (1992) 560.
[25] C. Fickert, R. Pikl, D. Gernet, S. Möller, W. Malisch, W. Kiefer, Fresenius J. Anal. Chem. 355 (1996) 340.
[26] G. Bringmann, U. Dauer, M. Lankers, J. Popp, U. Posset, W. Kiefer, J. Mol. Struc. 349 (1995) 431.
[27] S.-C. Chang, Z.H. Kafafi, R.H. Hauge, W.E. Billups, J.L. Margrave, J. Am. Chem. Soc. 107 (1985) 1447.
[28] A. Davison, J.A. McCleverty, G. Wilkinson, J. Chem. Soc. (A) (1963) 1133.
[29] (a) V.K. Dioumaev, J.F. Harrod, Organometallics 15 (1996) 3839. (b) X.-L. Luo, G.J. Kubas, C.J. Burns, J.C. Bryan, C.J. Unkefer, J. Am. Chem. Soc. 117 (1995) 1159.
[30] R.J.H. Clark, in: R.J.H. Clark, R.E. Hester (Eds.), Advances in Infrared and Raman Spectroscopy, vol. 1, Heyden, London, 1975, p. 143.
[31] M. Vitale, K.K. Lee, C.F. Hemann, R. Hille, T.L. Gustafson, B.E. Bursten, J. Am. Chem. Soc. 117 (1995) 2286.
[32] C. Fickert, P. Günther, P. Scholz, D. Gernet, R. Pikl, W. Kiefer, Inorg. Chim. Acta 251 (1996) 157.